Molecular Structure of Chloro-dodecafluorosubphthalocyanato Boron(III) by Gas-Phase Electron Diffraction and Quantum Chemical Calculations

S. Samdal* and H. V. Volden

Department of Chemistry, University of Oslo, P.O. Box 1033, Blindern, NO-0315 Oslo, Norway

V. R. Ferro and J. M. García de la Vega

Departamento de Química Física Aplicada, Universidad Autónoma de Madrid, 28049 Madrid, Spain

D. González-Rodríguez and T. Torres

Departamento de Química Orgánica, Universidad Autónoma de Madrid, 28049 Madrid, Spain

Received: February 8, 2007; In Final Form: March 8, 2007

The molecular structure of the chloro-dodecafluorosubphthalocyaninato boron(III) (F-SubPc) was determined with use of Gas Electron Diffraction (GED) and high-level quantum chemical calculations. The present results show that the F-SubPc molecule has a cone-shaped configuration, isoindole units are not planar, and the pyrrole ring has an envelope conformation. The structure parameters in the gas phase are determined. Some structural details can be observed such as the dihedral angle about the bond connecting the pyrrole ring and the benzene ring being ca. 174°. High-level theoretical calculations with several extended basis sets for this molecule have been carried out. The calculations are in very good agreement with experimental methods: X-ray and GED. Nevertheless, some disagreements particularly related to the B−Cl bond distance found in GED are discussed. Vibrational frequencies were computed obtaining eight values below 100 cm^{-1} and three bending potentials were examined. They suggest that this molecule is very flexible.

Introduction

The compound with molecular formula $C_{24}BClF_{12}N_6$, systematic name chloro[1,2,3,4,8,9,10,11,15,16,17,18-dodecafluoro-7,12:14,19-diimino-21,5-nitrilo-5*H*-tribenzo[*c*,*h*,*m*][1,6,11]-triazacyclopentadecinato (2-)κN22,κN23,κN24] boron(III) and trivial name chloro-dodecafluorosubphthalocyanato boron(III), abbreviated to F-SubPc, has been studied by gas-phase electron diffraction and high-level quantum chemical calculations.

Subphthalocyanines (SubPcs) are formed by three isoindole moieties coupled through nitrogen atoms and containing boron as the central atom, which also coordinates to another atom in the axial position, in this case a Cl atom (Figure 1). The preparation and the properties of these subporphyrinoids have recently been reviewed.[1,2] In recent years, a number of peripheral and axial substituted derivatives and other related compounds have been prepared. This growing activity is related to their chemical and thermal stabilities, their excellent photophysical[3−6] and nonlinear optical[7−11] properties, and their potential applications in molecular electronics, optoelectronics, and photonic technologies as, for example, in high-speed optical storage applications.[12] Moreover, SubPcs are also useful as synthetic precursors of their parent unsymmetrical substituted phthalocyanines.[13] Structural modifications of these compounds and some novel applications have also been reported.[14−16]

X-ray diffraction investigations[1] and theoretical calculations[17−21] have established the cone-shaped configuration of the SubPc macrocycle (Figure 1), i.e., the coordination at the boron atom is tetrahedral with a pyramidal $ClBN_3$ fragment and the isoindole moieties make the whole molecule resemble a cone. Although these molecules are nonplanar, they show a delocalized π electron system that is similar to that present in their higher homologues, i.e., the phthalocyanines.[14−16] The electronic UV−visible spectra of the SubPcs are similar in shape to those of the phthalocyanines with the Q-band shifted by about 100 nm to the shorter wavelength in comparison with phthalocyanines. An additional contribution to this picture was made[22] when it was shown that the SubPcs are nonlinear quasiplanar octupolar systems with permanent polarity, and that the behavior of the low-energy excited states responsible for the Q optical absorption band is very similar to that shown by planar π-conjugated octupoles with D_{3h} symmetry, but having a permanent dipole moment.

Spectroscopic and electrochemical features as well as some other properties and the X-ray structure of the SubPcs remain practically invariable under some diverse situations, such as peripheral and axial substitutions, one or two electron redox processes, and even electron excitation. These characteristics suggest that the molecular structure of the SubPcs does not undergo significant changes for these transformations. This is in good agreement with theoretical calculations,[17−21] which show that the geometrical parameters of the macrocyclic core for different isomers and derivatives of the SubPcs compounds are little influenced by substitution, and have only a small influence on the geometry and the electronic structure of the SubPc framework. Due to these results, the idea that the SubPc macrocycles are very stable and also rigid structures has been consolidated.

However, some new findings[23−29] indicate that the SubPcs are flexible molecules, present a rotational movement, and show

* Address correspondence to this author. E-mail: svein.samdal@kjemi.uio.no. Phone: 47-2285-5458. Fax: +47-2285-5441.

10.1021/jp0710988 CCC: $37.00
Published on Web 04/21/2007

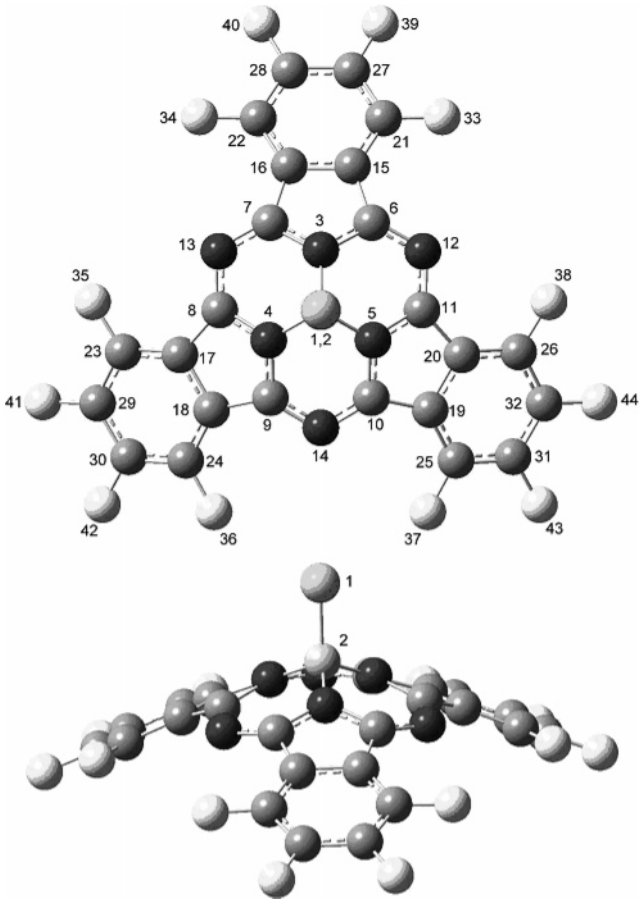

Figure 1. Numbering of the atoms for F-SubPc. The top figure shows the view from above the molecule along the B2−Cl1 bond, and the bottom figure shows a sidewise view of the molecule.

high mobility. That is why it is necessary to re-examine the ideas about the structure of the SubPc macrocycles described in the previous paragraph.

GED is the only experimental technique that can give information about the molecular structure in the gas phase for such large molecules. One limitation would be related to the vaporization of the sample without decomposition. However, adsorbed thin films of SubPcs have been prepared under vacuum and ultrahigh vacuum conditions,[30,31] by vapor deposition on a substrate,[32] and by sublimation[26] without destroying the molecular arrangement. Sublimation under extreme conditions (10^{-4} Torr and 350 °C) has been used for eliminating the halogen generated from BX_3 (X = F, Cl) and $PhBCl_2$ during the synthesis of the corresponding nonsubstituted SubPcs.[33] GED has previously been used to investigate some metal phthalocyanines,[34,35] indicating that SubPcs also could be investigated successfully by GED.

The main propose of this investigation is to determine the molecular structure of a SubPc molecule, F-SubPc, in the gas phase for comparison with its structure in the solid state and do high-level quantum chemical calculations to support the GED investigation and to gain more information about the flexibility of the molecule.

Experimental Section

Synthesis. The F-SubPc studied in the present work was synthesized as reported previously.[36] Boron trichloride (2 mL, 1 M solution in *p*-xylene) was added to the dry phthalonitrile precursor (2 mmol) under argon atmosphere. The reaction mixture was stirred under reflux for 20 min. The purple solution was then flushed with argon and the solvent was evaporated under vacuum. The resulting solid was subjected to silica gel column chromatography with hexane/ethyl acetate (3/1, v:v) as eluent. F-SubPc was isolated as a magenta solid (319 mg, 74%) with physical characteristics that are identical to those already described.[36]

Gas Electron Diffraction. The gas electron diffraction (GED) data were recorded on the Balzers KD-G2 unit[37] at the University of Oslo with use of an accelerating voltage of about 42 kV and a high-temperature stainless steel inlet system.[38,39] The experimental data were recorded on FujiFilm BAS-III image plates, and they were scanned with a FujiFilm BAS-1800II scanner. The image plate has a rectangular shape of approximately 13×18 cm^2. The data are collected and averaged over sectors along the positive and negative *y*-axis (short axis) and *x*-axis (long axis). The image plates are more sensitive, have higher resolution, much higher linear response, and a larger dynamic range compared to photographic plates. Due to the highly linear response of the image plates no blackness correction is necessary. More details about handling[40] of the experimental data and their processing[41] are given elsewhere.

The measured temperature represents the oven temperature, and is measured with a Cu/Constantan thermocouple. The thermocouple is placed outside the metal oven, and the dimension of the oven is approximately $7 \times 2 \times 2$ cm^3. The nozzle opening is connected to the oven and is approximately 4 cm from the thermocouple. The measured oven temperature is assumed to be the sample temperature as the gas.

The necessary modification and scattering functions were computed from tabulated atomic scattering factors[42] for the proper wavelength and *s*-values. The experimental backgrounds were computed with the program KCED12,[43] where the coefficients of a chosen degree of a polynomial function are determined by the least-squares method by minimizing the differences between the experimental intensity and the currently best geometrical model on the modified form. A background is subtracted from data obtained for each individual sector. An average experimental intensity curve is obtained along the *y*- and *x*-axis giving two average experimental intensity curves for each camera distance as shown in Figure 3. The experimental conditions are summarized in Table 1.

Quantum Chemical Calculations

The quantum chemical calculations were performed mostly with the Gaussian03 program package[44] running on the HP "superdome" facilities in Oslo. Several methods such as HF, MP2, and DFT were used with basis sets such as 6-31G*,[45] 6-311G**,[46,47] 6-311++G**,[47,48] and cc-pVTZ.[49] The functional used for the DFT calculations was the Becke three-parameter (B3LYP) hybrid functional,[50,51] which has been widely used in theoretical studies of pyrrole macrocycles.[17−21,52−58] To our knowledge, the present calculations represent the highest level performed so far on SubPc molecules. The molecular geometry was optimized assuming C_{3v} symmetry. The numbering of the atoms is shown in Figure 1. Additionally, a fragment of the molecule with some auxiliary points is shown in Figure 2.

Molecular force field calculations were carried out to ensure that the stationary points represent a local minimum, and to calculate the root-mean-square amplitude of vibrations, *u*-values, and correction coefficients used for shrinkage correction in the GED analysis. The molecular geometry obtained from some of the quantum chemical calculations is given in Table 2 and the calculated frequencies are given in Table 3.

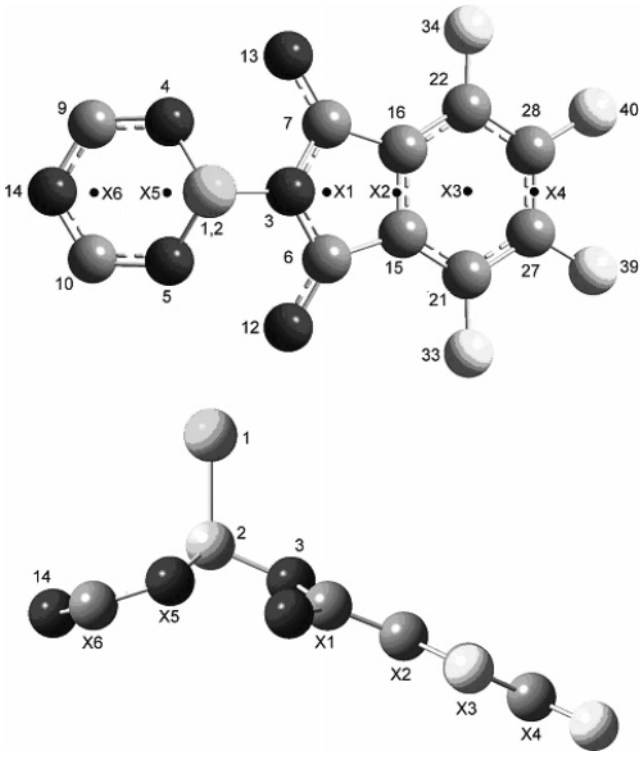

Figure 2. The upper figure shows auxiliary points which are located in the *xz*-symmetry plane and the molecular fragment is a projection onto the *xy*-plane. The lower figure is the projection of the molecular fragment on the *xz*-plane where the auxiliary points X are hidden behind the atoms in front. The coordinates are taken from the B3LYP/cc-pVTZ optimized structure.

Electron Diffraction

A brief description of the electron diffraction method is given which is relevant for a reader not an expert in the field in order to understand the assumptions made in this investigation, to understand the precision and accuracy obtained for the structure parameters, and to judge the experimental results.

The modified molecular intensity is the theoretical counterpart to the experimental measured intensity. It is given as[59]

$$I(s) = \text{scale constant} \sum n_{ij} g_{ij/kl}(s) \exp(-{}^1/_2 u_{ij}{}^2 s^2) \sin[(r_{ij} - \kappa_{ij} s^2)s] r_{ij}{}^{-1} \quad (1)$$

The sum is over all different distances r_{ij} between atoms i and j in the molecule. n_{ij} is the multiplicity of distances r_{ij}. u_{ij} is the root-mean-square amplitude of vibration and is calculated from the molecular force field usually obtained from quantum chemical calculations. κ_{ij} is an asymmetry constant usually very small and ignored. However, for bond distances the asymmetry constant κ_{ij} can be estimated from the formula[60] $\kappa_{ij} \approx a_3 u_{ij}{}^4/6$ where the parameter a_3 can be estimated from diatomic molecules[61] and usually has a value of about 0.02 pm^{-1}. s is a scattering parameter given as $s = 4\pi\lambda^{-1} \sin({}^1/_2\theta)$, where θ is the scattering angle. $g_{ij/kl}(s)$ is given as

$$g_{ij/kl}(s) = (|f_i(s)|\ |f_j(s)|)(|f_k(s)|\ |f_l(s)|)^{-1} \cos(\eta_i(s) - \eta_j(s)) \quad (2)$$

where $|f_i(s)|$ is the absolute coherent scattering factor of atom i and η_i is the phase of the complex atomic scattering factor of atom i. The atoms k and l are fixed and they are usually selected as those bond atoms which contribute most to the molecular intensity, in this case $k = l = C$. The experimental data are transformed to intensities corresponding to the modified molecular intensity. All distances r_{ij} are calculated from a set of independent molecular parameters as specified in Table 4. These parameters are adjusted by using the least-square method to obtain the best fit between the experimental and theoretical modified molecular intensities. It should be noted that the modified molecular intensity essentially represents a sum of damped sinus waves of the form $\sin(r_{ij}s)$. Moreover closely spaced bond distances will inevitably be difficult to determine accurately. For this reason, some assumptions based on the quantum chemical calculations have been made for F-SubPc. The assumption made in the present work is that the difference between those closely spaced bond distances are fixed to the difference calculated by the quantum chemical calculations.

$g_{ij/kl}(s)$ can be estimated to be Z_iZ_j/Z_kZ_l, where Z is the atomic number. The relative contribution to the molecular intensity for atom pairs involving light atoms is smaller than that for those involving heavier atoms, and inevitably reduced precision and accuracy are obtained for those distances. This can especially be seen for the B−Cl bond distance as the tiny peak located at 193 pm on the RD-curve in Figure 4. The B−Cl bond has low multiplicity and contains a light B atom.

r_a are structure parameters obtained by fitting the bond distances to eq 1; however, these parameters do not give a consistent geometry. This was first discovered for linear fragments.[62−64] As an example, in a GED experiment the r(O···O) in CO_2 is not exactly equal to $2r$(C═O) but slightly shorter. This is called the shrinkage effect, which is due to the thermal motion of the atoms and was first explained by

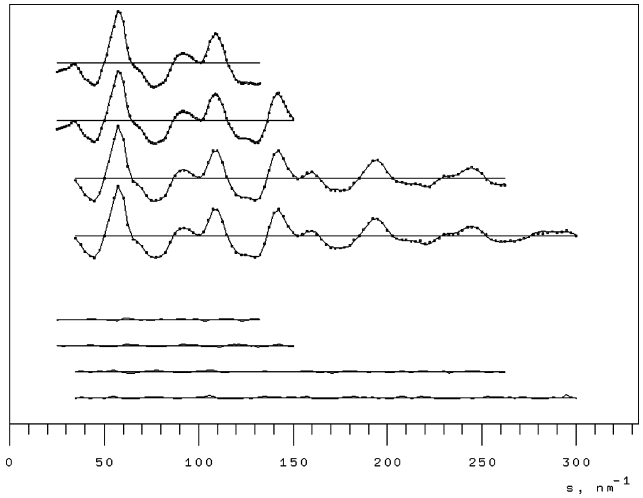

Figure 3. The two first curves show the average modified molecular intensity curves from all sectors in the *y*- and *x*-direction for the long camera distance, respectively, and the next two curves show the corresponding curves for the short camera distance. Full line curves are theoretical modified intensity curves obtained for the best model (Table 4, scheme 1). The four curves on the bottom are difference curves.

TABLE 1: Experimental Conditions for the ED Study of the F-SubPc

	long camera	middle camera
ambient temp/K	576−577	586−588
nozzle-to-plate distance/mm	498.39	248.92
no. of plates	3	4
s-limits: x-/y-direction/nm^{-1}	25.0−150.0/ 25.0−132.5	35.0−300.0/ 35.0−262.5
$\Delta s/nm^{-1}$	1.25	2.50
accelerating voltage/kV	42	42
electron wavelength/pm	5.82	5.82
degree of polynomial[a]	10	11

[a] Degree of polynomial used in the background subtraction.

TABLE 2: Quantum Chemical Calculations for F-SubPc[a]

	F-Sub (C_{3v})						F-isoindole (C_{2v})	pyrrole (C_{2v})
parameter	B3LYP 6-31G*	HF 6-311G**	MP2(FC) 6-311G**	B3LYP 6-311G**	B3LYP 6-311++G**	B3LYP[b] cc-pVTZ	B3LYP cc-pVTZ	B3LYP cc-pVTZ
bond distances								
B2−Cl1	186.7	186.2	182.3	186.7	186.4	186.57		
B2−N3	149.1	148.3	149.3	149.1	149.2	148.97		
N3−C6	136.7	134.7	136.8	136.7	136.7	136.40	136.4	137.1
C6−N12	133.6	132.0	134.5	133.6	133.6	133.41		
C6−C15	145.4	145.2	145.5	145.4	145.5	145.19	138.7	137.3
C15−C16	143.3	141.2	143.4	143.3	143.3	143.03	144.5	142.1
C15−C21	139.0	138.5	139.3	139.0	139.0	138.71	141.1	
C21−C27	138.9	136.8	139.5	138.9	138.9	138.65	136.2	
C27−C28	140.1	139.5	140.5	140.1	140.1	139.92	142.6	
C21−F33	133.2	130.7	133.0	133.2	133.3	132.97	134.3	
C27−F39	133.3	130.9	133.0	133.3	133.2	133.00	133.8	
angles								
Cl1−B2−N3	113.8	114.1	114.5	113.8	113.9	113.9		
B2−N3−C6	122.4	122.2	122.6	122.4	122.4	122.4		
C6−N3−C7	114.1	114.6	114.0	114.1	114.0	114.1	112.3	109.8
N3−C6−N12	122.7	122.7	123.1	122.7	122.7	122.6		
N3−C6−C15	105.1	104.9	105.2	105.1	105.1	105.1	106.7	107.7
N12−C6−C15	130.7	130.9	129.8	130.7	130.7	130.8		
C6−C15−C16	107.2	107.1	107.2	107.2	107.2	107.2	107.2	107.4
C16−C15−C21	120.2	120.3	120.4	120.2	120.1	120.1	119.4	125.7
C15−C21−C27	118.9	118.6	118.5	118.9	119.1	119.0	119.5	
C21−C27−C28	121.0	121.1	121.1	121.0	120.9	120.9	121.0	
C15−C21−F33	121.8	121.6	121.9	121.8	121.8	121.7	120.0	
C21−C27−F39	120.2	120.4	120.1	120.2	120.2	120.2	121.2	
C6−N12−C11	117.4	117.8	116.3	117.4	117.5	117.6		
dihedral angles								
Cl1−B2−N3−C6	96.5	96.2	95.6	96.5	96.5	96.4		
B2−N3−C6−N12	12.9	13.1	14.3	12.9	13.0	13.0		
B2−N3−C6−C15	179.9	−179.5	−179.8	179.9	−179.9	−179.9	180.0	
N3−C6−C15−C16	−6.8	−6.8	−6.0	−6.8	−6.9	−6.8	0.0	
N12−C6−C15−C16	158.8	159.2	158.6	158.8	158.8	158.9	180.0	
N3−C6−C15−C21	178.1	177.8	178.1	178.1	177.9	178.1	180.0	
C6−C15−C21−C27	175.6	175.9	176.4	175.6	175.7	175.6	180.0	
C6−C15−C21−F33	−4.9	−4.6	−4.2	−4.9	−4.9	−4.9	0.0	
C15−C21−C27−C28	−1.0	−1.0	−0.9	−1.0	−0.9	−1.0	0.0	
C15−C21−C27−F39	178.9	179.0	178.9	178.9	178.8	178.9	180.0	
C21−C15−C16−C22	0.0	0.0	0.0	0.0	0.0	0.0	0.0	
C21−C27−C28−C22	0.0	0.0	0.0	0.0	0.0	0.0	0.0	
C16−C15−C21−C27	1.0	1.0	0.9	1.0	0.9	1.0	0.0	
C16−C15−C21−F33	−179.5	−179.6	−179.7	−179.5	−179.7	−179.6	180.0	
C6−C15−C16−C7	0.0	0.0	0.0	0.0	0.0	0.0	0.0	

[a] For numbering of the atoms see Figures 1 and 2. Distances in pm and angles in deg. [b] Some auxiliary angles are given for this basis set: B2−N3−X2 = 170.0°, N3−X1−X2 = 167.9°, X1−X2−X3 = 175.9°, B2−X5−X6 = 156.2°, and N14−X6−X5 = 173.4°.

Morino.[65,66] The shrinkage effect can be corrected for by using either a rectilinear[67,68] or a curvilinear[69,70] treatment of the vibrating atoms. This investigation has tested both these models. The program SHRINK[69,70] was used to calculate these shrinkage correction terms (k_{h0} and k_{h1}), the root-mean-square amplitudes of vibrations (u), and the $r_a - r_e$ differences from the molecular force field.

Structure Analysis

According to all of our force field calculations the molecule possesses C_{3v} symmetry, and this symmetry has been assumed throughout the GED analysis. Thus, the whole molecule can be generated from the fragment shown in Figure 2 by rotating 120° and 240° about the B2−Cl1 bond axes

To simplify the description of the molecular geometry the fluoro-substituted benzene fragment is assumed planar, i.e., the atoms C15, C16, C21, C22, C27, C28, F33, F34, F39, and F40 are all in the same plane. According to the quantum chemical calculations no dihedral angles in the fluoro-substituted benzene fragment deviate more than 1° (see Table 2) from their assumed values of either 0° or 180°. Therefore, this simplification should be justified. However, according to the quantum chemical calculations the dihedral angle C7−C16−C15−C21 differs from 180° and hence is used as an independent parameter. Moreover, the quantum chemical calculations also indicate that the pyrrole ring has an envelope conformation, and the envelope angle, N3−X1−X2 (see Figure 2), is defined as the angle between the two planes given by the atoms C6, N3, C7 and the atoms C6, C15, C16, C7, i.e., the dihedral angle about C6···C7. This angle is also used as an independent parameter. Finally, the quantum chemical calculations show that the ring defined by the atoms B2, N4, C9, N14, C10, and N5 has a boat conformation. Therefore, the boat angle N14−X6−X5, i.e., the dihedral angle about C9···C10, is selected as an independent parameter. The other boat angle B2−X5−X6, i.e., the dihedral angle about N4···N5, is a dependent parameter and is calculated from the independent parameters. In summary, the following set of 16 independent parameters is used to describe the molecular geometry imposing C_{3v} symmetry: bond distances B2−Cl1, B2−N3, N3−C6, C9−N14 (equal to C6−N12), C6−C15, C15−C16, C15−C21, C27−C28, C21−F33, C27−F39

TABLE 3: Calculated Frequencies for F-SubPc with Use of B3LYP/6-311G and C_{3v} Symmetry[a]**

no.	specie	freq	IR int	no.	specie	freq	IR int
1	E	1668.9	17.1	43	E	669.6	7.1
2	A_2	1665.2	0.0	44	E	666.6	3.5
3	A_1	1636.4	0.4	45	A_2	665.7	0.0
4	E	1632.6	10.9	46	A_1	658.0	13.0
5	E	1553.3	311.0	47	E	645.8	0.4
6	A_2	1548.9	0.0	48	E	598.3	46.4
7	A_1	1525.7	20.6	49	E	580.4	39.6
8	E	1505.6	802.6	50	A_2	524.9	0.0
9	A_1	1498.3	244.3	51	E	509.6	0.7
10	E	1491.5	330.9	52	A_2	502.5	0.0
11	A_1	1479.5	46.6	53	A_1	480.8	0.07
12	A_2	1469.1	0.0	54	E	467.8	0.5
13	E	1468.8	29.5	55	A_2	430.7	0.0
14	E	1411.3	76.3	56	E	429.2	0.1
15	A_1	1400.1	0.01	57	A_1	418.5	23.0
16	E	1362.5	1.0	58	A_1	395.9	1.7
17	A_2	1330.0	0.0	59	E	387.6	1.1
18	E	1302.2	276.6	60	A_2	383.0	0.0
19	E	1285.5	15.8	61	E	372.5	1.1
20	A_1	1273.3	9.6	62	A_1	342.0	1.7
21	A_2	1257.4	0.0	63	E	324.1	1.9
22	E	1251.2	116.7	64	A_1	299.2	1.6
23	E	1192.7	30.0	65	E	297.9	0.7
24	A_1	1176.6	0.02	66	A_2	287.0	0.0
25	E	1137.5	326.6	67	E	282.6	0.7
26	A_2	1120.6	0.0	68	A_1	278.8	0.06
27	E	1083.6	10.9	69	E	277.9	0.2
28	A_1	1068.1	164.0	70	E	247.0	1.5
29	E	982.2	190.2	71	A_1	220.9	0.05
30	A_2	974.7	0.0	72	E	200.3	1.6
31	E	899.1	34.2	73	A_1	197.3	1.9
32	A_1	852.6	191.1	74	E	162.7	0.03
33	E	850.0	5.9	75	A_2	159.0	0.0
34	A_2	820.1	0.0	76	E	149.7	0.4
35	E	781.6	4.6	77	A_2	143.7	0.0
36	A_1	767.6	0.1	78	A_1	118.0	0.05
37	E	748.7	34.0	79	E	112.1	0.3
38	A_1	734.0	69.4	80	E	83.8	0.01
39	A_2	722.5	0.0	81	E	61.1	0.4
40	E	722.4	7.6	82	A_2	53.4	0.0
41	A_2	685.3	0.0	83	E	31.3	0.003
42	A_1	675.9	73.3	84	A_1	28.3	0.07

[a] Frequencies in cm^{-1} and IR intensities in kM/mol.

and angles Cl1−B2−N3, C6−N3−C7, C15−C21−C27, N3−X1−X2, X1−X2−X3, and N14−X6−X5.

As explained before the GED method is not very accurate for determining individual bond lengths when several bond lengths of approximately the same magnitude are present. Therefore, some assumptions concerning the bond distances must be made. As seen from Table 2, the differences between the calculated bond lengths are more or less independent of the method and the basis set. We have therefore assumed the differences $\Delta(C-F) = r(C27-F39) - r(C21-F33) = 0.03$ pm, $\Delta(C-N) = r(C6-N12) - r(N3-C6) = -2.99$ pm, and $\Delta(C-C) = r(C21-C27) - r(C15-C21) = -0.06$ pm to be equal to the differences obtained from the B3LYP/cc-pVTZ calculation.

The final results are shown in Table 4. The modified molecular intensity curves corresponding to the best fit (see the column labeled scheme 1 in Table 4) are shown in Figure 3, whereas the corresponding radial distribution curves are shown in Figure 4.

Results and Discussion

Optimized Theoretical Geometry. The optimized geometries from the quantum chemical calculations are presented in Table 2. All calculated bond angles and dihedral angles are surprisingly consistent and more or less independent of both the method and the basis set used. This is also the case for the bond distances except for the HF/6-311G** calculation where most of the bond distances are calculated shorter than for the other methods as expected. It should also be noted that the B−Cl bond distance obtained from the MP2(FC)/6-311G** calculation is considerably shorter than the value obtained by the other methods and basis sets, as well as compared with the experimentally obtained values given in Table 4. Three important structural features are predicted by all of our calculations: (1) the pyrrole ring has an envelope conformation in which the envelope angle N3−X1−X3 (equal to the dihedral angle N3−C6−C7−C16) is 168.0°, (2) the six-membered rings as specified by the atoms B2N4C9N14C10N5 form a boat conformation, where the two boat angles N14−X6−X5 (equal to the dihedral angle N14−C9−C10−N5) and B2−X5−X6 (equal to the dihedral angle B2−N4−N5−C10) are 173.4° and 156.2°, respectively, and (3) the C6−C15−C16−C7 fragment in the pyrrole ring is not coplanar with the benzene fragment giving a X1−X2−X3 angle (equal to the dihedral angle C6−C15−C16−C22) of 175.9°. The given values are from the B3LYP/cc-pVTZ calculation. These findings are also found experimentally as seen in Table 4.

Molecular Vibrations and Flexibility. All force field calculations confirm that F-SubPc has C_{3v} symmetry, and therefore the normal modes belong to the following symmetry species: $23A_1 + 19A_2 + 42E$. The vibrational frequencies belonging to A_1 and E irreducible representations are active while A_2 modes are inactive in both IR and Raman. The unscaled B3LYP/6-311G** frequencies are given in Table 3, and this molecular force field is used to calculate the *u*-values and the correction terms for shrinkage correction in the GED analysis. Some of the *u*-values are given in Table 5. It should be noted that there are eight vibrational modes (three degenerate) giving five different frequencies below 100 cm^{-1}. This clearly indicates than we are dealing with a very flexible molecule as suggested previously.[23−29] The eight lowest frequency modes can be best described as follows: a breathing mode (A_1, 28 cm^{-1}), which resembles a gel fish swimming motion, a breathing motion of two isoindole units and a twisting of the third (E, 31 cm^{-1}), a twisting of the three isoindole units as a propeller (A_2, 53 cm^{-1}), a twisting of two isoindole units and bending of the third (E, 61 cm^{-1}), and a similar movement for the 84 cm^{-1} E-mode. Other vibrational modes of special interest related to the flexibility of the molecule would be the movement of the $ClBN_3$ fragment, which could be described as an inverted umbrella struggling to obtain its normal form. This inverted umbrella motion appears at 419 cm^{-1} (A_1) and the B−Cl stretching frequency appears at 853 cm^{-1} (A_1).

A B3LYP/6-31G* calculation placing the B atom in the middle of the N_3 cavity and all other atoms in the *xy*-plane (i.e., forcing the macrocycle to planarity) except the Cl atom, which is located above the B atom, is 210 kJ/mol less stable than the optimized nonplanar geometry. However, even more important, the calculation predicts that the B−Cl bond distance increases from 186.6 pm to 265.4 pm. This strongly indicates that the B−Cl bond length changes considerably during the breathing motion (A_1, 28 cm^{-1}).

Since the question of the flexibility of the molecule has been raised, it will be of interest to explore this further particularly related to the isoindole fragment. In this sense, it is important to note that the line through B2−N3−X1−X2−X3−X4 has a zigzag pattern, and that the envelope angle N3−X1−X2 (dihedral angle N3−C6−C7−C16) is 167.9°. Regarding this

TABLE 4: Experimental Results for F-SubPc[a]

parameter	scheme 1	scheme 2[b]	scheme 3[c]	r_e(GED)[d]	r_e(B3LYP/ cc-pVTZ)	X-ray[e]
Cl1−B2	192.7(34)	195.5(36)	195.4(36)	191.7(34)	186.6	186.6(4)
B2−N3	146.4(18)	146.2(27)	146.3(27)	145.9(18)	149.0	148.5 (147.7/149.4)
N3−C6	136.7(9)	136.7(8)	136.6(8)	136.6(9)	136.4	137.0 (136.4/137.6)
Δ(C−N)[f]	−2.99	−2.99	−2.99		−2.99	−2.0
C6−C15	145.0(18)	144.0(17)	144.0(17)	144.5(18)	145.2	145.7 (145.2/146.2)
C15−C16	143.0(41)	147.0(40)	146.9(39)	142.5(41)	143.0	142.7 (142.4/143.4)
C15−C21	139.2(8)	138.6(20)	138.5(20)	138.7(8)	138.7	138.4 (138.1/139.1)
(C−C)[g]	−0.06	−0.06	−0.06		−0.06	−0.5
C21−F33	134.9(8)	134.6(8)	134.6(8)	134.2(8)	133.0	134.4 (134.1/135.0)
(C−F)[h]	0.03	0.03	0.03		0.03	0.0
Cl1B2N3	108.7(21)	109.0(23)	109.1(22)		113.9	113.4 (112.5/114.4)
C6N3C7	109.8(19)	110.5(21)	110.7(22)		114.1	113.4 (113.2/113.9)
B2N3X1	158.3(44)	159.8(57)	160.0(62)		170.0	166.4 (164.6/169.3)
N3X1X2	168.0(40)	163.7(45)	164.5(44)		167.9	167.6 (166.0/169.3)
C16C15C21	120.1(10)	119.0(13)	119.2(13)		120.1	119.8 (118.8/120.6)
X1X2X3	174.1(51)	181.4(67)	181.3(66)		175.9	176.0 (172.0/179.3)
C15C21C27	117.8(14)	119.9(31)	119.8(30)		119.0	119.3 (119.0/119.6)
C15C21F33	120.2(12)	119.7(13)	119.8(13)		121.7	120.8 (120.3/121.3)
C28C27F39	118.6(17)	118.3(24)	118.5(21)		118.9	118.8 (118.3/119.4)
N14X6X5	174.0(58)	172.8(69)	173.2(68)		173.4	172.8 (170.9/175.4)
R_f, %	4.52	4.61	4.61			

[a] Distances (r_a) in pm and angles in deg. Parenthesized values are estimated error limits given as $2.5(\sigma^2_{lsq} + (0.001r)^2)^{1/2}$ for bond distances, where σ_{lsq} is one standard deviation obtained from the least-squares refinement by using a diagonal weight matrix and the second term represent 0.1% uncertainty in the electron wavelength. The error estimates are in units of the last digits. Goodness of fit, R_f (%), defined as $\sum_s w(I_s^{obs} - I_s^{calc})^2/\sum_s w(I_s^{obs})^2$, where w is a weight function usually equal to 1. The largest correlation coefficients (>0.70) are between the following parameters: C6−C15/C15−C16 = −0.84, N3−C6/C21−F33 = −0.70, N3−C6/C6N3C7 = −0.74, C6−C15/C16C15C21 = 0.80, C15−C16/ C16C15C21 = −0.86, Cl1B2N3/B2N3X1 = 0.76, C16C15C21/C15C21C27 = −0.81. [b] r_a is transferred to r_{h0}, shrinkage corrected, and transferred back to r_a. [c] r_a is transferred to r_{h1}, shrinkage corrected, and transferred back to r_a. [d] The $r_a - r_e$ differences are from the SHRINK program. [e] Average values from X-ray[15] and parenthesized values (min/max) correspond to the smallest and largest value respectively. [f] Δ(C−N) = r(C6−N12) − r(N3−C6). [g] Δ(C−C) = r(C21−C27) − r(C15−C21). [h] Δ(C−F) = r(C27−F39) − r(C21−F33).

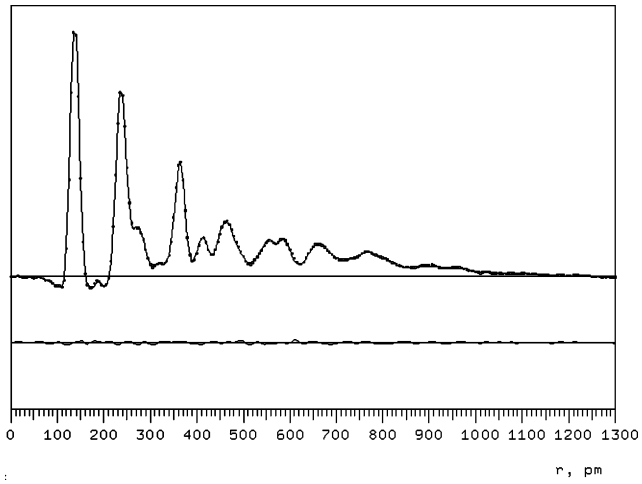

Figure 4. The upper curves are the experimental (dots) and theoretical (full line) radial distribution curves for F-SubPc. The theoretical data from the best model (Table 4, scheme 1) were used for the unobserved region $s < 25.0$ nm^{-1}. The damping coefficient for the radial distribution function is 25 pm.[2]

TABLE 5: Some Root-Mean-Square Amplitudes of Vibration (u) Refined in Groups[a]

group	atom pair	N_o	distance	u(GED)	u_{h0}[b]	u_{h1}[c]
1	F39···F40	7	264	15.1(6)	13.3	13.3
	B2···N12		285	9.4	7.6	7.6
2	C6···F33	3	307	9.7(17)	12.2	12.1
	N12···C21		328	8.7	11.2	11.2
3	C6···N13	13	344	6.6(5)	7.0	6.9
	C6···C27		380	7.21	7.6	7.5
4	C6···C8	8	395	7.6(13)	7.9	7.8
	N3···F33		435	10.9	11.2	11.0
5	C6···C19	17	446	8.6(14)	8.3	8.2
	B2···C21		501	8.7	8.4	8.3
6	N3···C23	10	528	12.4(12)	11.2	11.0
	C6···C18		554	11.6	10.4	10.3
7	C21···F38	11	553	30.7(12)	29.3	28.9
	B2···C27		602	10.0	8.6	8.3
8	C21···C26	18	607	25.2(17)	23.0	22.8
	Cl1···C27		706	25.1	22.9	22.6
9	C15···C25	4	701	18.3(32)	15.1	14.9
	C21···C32		740	29.8	26.7	26.4
10	F33···F44	23	740	39.9(47)	37.4	36.7
	C27···C32		870	35.0	31.9	31.5

[a] The root-mean-square amplitudes of vibration are refined in groups where the first atom pair corresponds to the shortest distance in the group and the second pair corresponds to the largest distance in the group. N_o is the total distance in the group. The starting values are the calculated values and all amplitudes get the same shift and standard deviation. Parenthesized values are estimated error limits given as 2.5 times the least-squares standard deviation. [b] Rectilinear treatment of the vibrating atoms. [c] Curvilinear treatment of the vibrating atoms.

topic, several questions immediately arise: What does the envelope puckering potential (the potential energy as a function of the bending angle N3−X1−X2 of the "envelope") look like? Will the puckering potential be symmetric or unsymmetric, or will the puckering potential have a barrier at the planar arrangement of the pyrrole ring and thereby create the possibility for another conformation? To explore this, we have used the Z-matrix optimizing procedure in which the structure has been optimized for fixed values of the pyramidalization angle B2−N3−X1 = (90 + $a1$)°, the envelope angle N3−X1−X2 = (90 + $a2$)°, and the pyrrole−benzene angle X1−X2−X3 = (90 + $a3$)°. All calculations have been constrained to C_{3v} symmetry and with the B3LYP/6-31G* computational method. All parameters except for the fixed ones have been fully optimized. The bending potentials are shown in Figure 5, where the angles $a1$, $a2$, $a3$ have been used to describe the bending potential. It is quite clear that the bending potentials are rather symmetric and there are no indications of more than one conformation. It

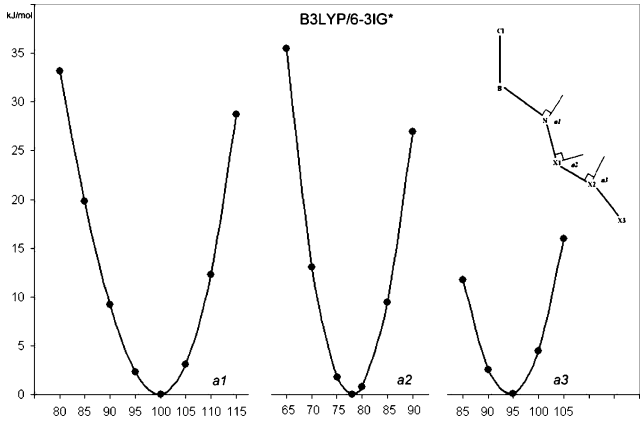

Figure 5. Bending potentials. The first bending potential (*a*1) represents the bending of the B2−N3 bond against the C6N3C7 plane, i.e., inverted umbrella motion of the N3 atom. The second bending potential (*a*2) represents the envelope puckering potential of the pyrrole ring, i.e., the bending angle N3X1X2 or the dihedral angle about C6••C7. The third bending potential (*a*3) represents the bending of the pyrrole ring against the benzene ring, i.e., the bending angle X1X2X3 or the dihedral angle about the C15−C16 bond.

is interesting to notice that the energy required to obtain a planar configuration about the N3 atom is 9.2 kJ/mol (to make the angle B2−N3−X1 = 180°, i.e., *a*1 = 90°, see Figure 5), while 26.9 kJ/mol is required to obtain a planar pyrrole ring (to make the angle N3−X1−X2 = 180°, i.e., *a*2 = 90°, see Figure 5). To make the pyrrole ring completely coplanar with the benzene ring, only 2.6 kJ/mol (to make the angle X1−X2−X3 = 180°, i.e., *a*3 = 90°, see Figure 5) is required.

Experimentally Derived Structure. The experimentally derived structure parameters are given in Table 4 together with their theoretical counterparts. Three different refinement schemes have been used, scheme 1 in which no shrinkage correction is made, scheme 2 in which the rectilinear approach has been used for the shrinkage correction, and scheme 3 in which the curvilinear approach has been used for the shrinkage correction. The curvilinear approach, scheme 3, represents a more conceptionally appealing physical model. The contribution from the B−Cl bond distance to the total modified intensity is rather small: see the tiny peak in the RD-curve (Figure 4) located at 193 pm. The least-squares method minimizes the least-squares sum and thereby also decreases the goodness-of-fit factor, R_f. This might be at the expense of the small peak at 193 pm because of its small contribution. This is exactly what happens for schemes 2 and 3. The RD-curves, not shown, for schemes 2 and 3 clearly show that the peak of the theoretical RD-curve is shifted to the right compared to the experimental peak. This indicates that the derived B−Cl bond distance is too long for schemes 2 and 3. This is the main reason for selecting scheme 1 as our best model. However, a very careful examination of the peak located at 193 pm in Figure 4 shows that the theoretical RD-curve is slightly shifted to the right also when scheme 1 is used. Further, it should be emphasized that the GED structure represents an average structure that is averaged over all vibrational states. This might give particularly large differences between structural parameters derived from GED and ab initio if there are low-frequency modes that create anharmonic changes in some of the structure parameters. The bending potentials shown in Figure 5 are all rather harmonic. Schemes 2 and 3 are supposed to correct for vibrational effects; however, the theory is based on small-amplitude oscillations of the atoms from their equilibrium position, i.e., a rigid molecule. This is certainly not the case for this molecule and applying these corrections gives a slightly worse R_f factor. The most pronounced deviations in the structure parameters are found for B−Cl, C15−C16, and X1X2X3 for schemes 1, 2, and 3. The agreement with the quantum chemical calculated values is less for schemes 2 and 3 than for scheme 1. This may also support our selection of scheme 1 as our best model.

Generally, there is good agreement between the experimentally derived structure parameters using the GED method and the B3LYP/cc-pVTZ values as seen in Table 4. Compared with the calculated values there seems to be a significant difference between the experimental and calculated values for the parameters B−Cl, B−N, Cl−B−N, and C−N−C and the envelope angle B−N−X1. All these parameters are related to the central part of the SubPc unit, and this might indicate that either an even larger basis set has to be used to reproduce the experimental values, or that lack of proper vibrational corrections might influence the experimental determination of these structural parameters.

However, it is very important to bear in mind that the experimentally obtained structures may be different for different experimental methods and different from the quantum chemical calculations. The experimental structure derived from X-ray may be influenced by crystal packing forces and the location of the position of the atoms represents the centers of the electron density of the atoms. The r_a(GED) structure represents an average structure of the nuclei averaged over all vibrational states while the quantum chemical calculations give an equilibrium r_e structure. All these structures may be different and comparison should be made with caution. Comparison of the B3LYP/cc-pVTZ structure and the X-ray structure given in Table 4 shows a very good agreement indicating that the crystal packing forces are not strongly influencing the molecular structure and that the centers of the electron densities are close to the equilibrium positions of the atoms. Comparing the B3LYP/cc-pVTZ structure with the GED structure reveals considerably larger differences than with the X-ray structure, indicating that the average structure GED and the r_e structure are considerably different even after a correction from r_a to r_e. The elongation of the B−Cl bond length can be easily explained due to the thermal averaging over the vibrational state of the breathing (A_1, 28 cm^{-1}) motion. As previously mentioned, the B3LYP/6-31G* calculation for the "planar" molecule shows a considerable elongation of the B−Cl bond distance from 186.6 to 265.4 pm, and it is therefore expected the B−Cl bond length increases as the molecule flattens. The thermal averaging over all the vibrational excited states will therefore give a B−Cl bond distance longer than that for the ground state as is also observed by GED. The B−Cl bond distance in the vibrational ground state will be closer to the B−Cl bond distance obtained by quantum chemical calculations. The only way to avoid this problem would be to include a dynamic model simulating this motion, but this is not feasible for such a large molecule. Further, the structure parameters Cl1B2N3, C6N3C7, and B2N3X1 are all smaller than their calculated counterparts. A good explanation for this is not obvious but certainly a proper correction for the shrinkage effect, which is not yet theoretically available for such a flexible molecule, may cause some significant changes.

Most of the refined amplitudes given in Table 4 are within the experimental error of the calculated once except for the two first, and most likely this is due to the lack of a proper shrinkage correction and to the constraints applied to the structure parameters.

Concluding Remarks

The F-SubPc molecule has a cone-shaped configuration and the isoindole units are not planar. The pyrrole ring has an envelope conformation and the dihedral angle about the bond connecting the pyrrole ring and the benzene ring is not 180°. These features determine that the line through the positions B2, N3, X1, X2, X3, and X4 has a zigzag pattern (see Figure 2). Furthermore, the six-membered rings (as specified by the atoms B2, N4, C9, N14, C10, and N5) have a boat conformation. The structure determined in the solid state is in very good agreement with the high-level quantum chemical calculations, while some of the average structure parameters derived with the GED method disagree. An important disagreement related to the B−Cl bond distance and its elongation compared to the quantum chemical calculations and X-ray can be explained due to the thermal averaging of the B−Cl bond distance over vibrationally excited states for the breathing vibrational mode. Eight vibration frequencies (three degenerate) give five different frequencies below 100 cm^{-1} indicating a very flexible molecule. The major flexibility of the molecule is related to the central fragment of the molecule and to the movement of the isoindole units. The bending potentials along the B2−N3−X1−X2−X3−X4 axis are rather symmetric and there are no indications of more than one conformation.

Acknowledgment. S. Gundersen is acknowledged for work-up of the experimental data and creating some of the figures. The University of Oslo is thanked for a generous amount of computer time. The Spanish economical support of the present work was made through the MEC grants (CTQ-2005-08933-BQU, CTQ-2004-06615-BQU, and MAT-2004-03849) and the Comunidad de Madrid (S-0505/PPQ/ 000225).

Supporting Information Available: Cartesian coordinates (Å) corresponding to the numeration of atoms (see Figure 1) for the molecular structure of chlorododecafluorosubphthalocyanato boron(III) optimized at the B3LYP/cc-pVTZ level, Table S1. This material is available free of charge via the Internet at http://pubs.acs.org.

References and Notes

(1) Claessens, C. G.; Gonzalez-Rodriguez, D.; Torres, T. *Chem. Rev.* **2002**, *102*, 835.

(2) Torres, T. *Angew. Chem., Int. Ed.* **2006**, *45*, 2834.

(3) Gonzalez-Rodriguez, D.; Torres, T.; Guldi, D. M.; Rivera, J.; Herranz, M. A.; Echegoyen, L. *J. Am. Chem. Soc.* **2004**, *126*, 6301.

(4) Iglesias, R. S.; Claessens, C. G.; Torres, T.; Rahman, G. M. A.; Guldi, D. M. *Chem. Commun.* **2005**, 2113.

(5) Gonzalez-Rodriguez, D.; Claessens, C. G.; Torres, T.; Liu, S.; Echegoyen, L.; Vila, N.; Nonell, S. *Chem. Eur. J.* **2005**, *11*, 3881.

(6) Gonzalez-Rodriguez, D.; Torres, T.; Olmstead, M. M.; Rivera, J.; Angeles Herranz, M.; Echegoyen, L.; Atienza Castellanos, C.; Guldi, D. M. *J. Am. Chem. Soc.* **2006**, *128*, 10680.

(7) Sastre, A.; Torres, T.; Diaz-Garcia, M. A.; Agullo-Lopez, F.; Dhenaut, C.; Brasselet, S.; Ledoux, I.; Zyss, J. *J. Am. Chem. Soc.* **1996**, *118*, 2746.

(8) De la Torre, G.; Torres, T.; Agullo-Lopez, F. *Adv. Mater.* **1997**, *9*, 265.

(9) Rojo, G.; Agullo-Lopez, F.; del Rey, B.; Torres, T. *J. Appl. Phys.* **1998**, *84*, 6507.

(10) Del Rey, B.; Keller, U.; Torres, T.; Rojo, G.; Agullo-Lopez, F.; Nonell, S.; Marti, C.; Brasselet, S.; Ledoux, I.; Zyss, J. *J. Am. Chem. Soc.* **1998**, *120*, 12808.

(11) Claessens, C. G.; Gonzalez-Rodriguez, D.; Torres, T.; Martin, G.; Agullo-Lopez, F.; Ledoux, I.; Zyss, J.; Ferro, V. R.; Garcia de la Vega, J. M. *J. Phys. Chem. B* **2005**, *109*, 3800.

(12) Cao, W.-F.; Tu, H.-Y.; Wang, J.; Tian, H.; Wang, Y.; Gu, D.; Gan, F. *Dyes Pigm.* **2002**, *54*, 213.

(13) Sastre, A.; del Rey, B.; Torres, T. *J. Org. Chem.* **1996**, *61*, 8591. De la Torre, G.; Claessens, C. G.; Torres, T. *Chem. Commun.* In press. DOI: 10.1039/b614234f.

(14) Claessens, C. G.; Torres, T. *Angew. Chem., Int. Ed.* **2002**, *41*, 2561.

(15) Fukuda, T.; Stork, J. R.; Potucek, R. J.; Olmstead, M. M.; Noll, B. C.; Kobayashi, N.; Durfee, W. S. *Angew. Chem., Int. Ed.* **2002**, *41*, 2565.

(16) Palomares, E.; Martinez-Diaz, M. V.; Torres, T.; Coronado, E. *Adv. Funct. Mater.* **2006**, *16*, 1166.

(17) Ferro, V. R.; Poveda, L. A.; Claessens, C. G.; Gonzalez-Jonte, R. H.; Garcia de la Vega, J. M. *Int. J. Quantum Chem.* **2003**, *91*, 369.

(18) Gong, X. D.; Xiao, H. M.; Gao, P.; Tian, H. *THEOCHEM* **2002**, *587*, 189.

(19) Ferro, V. R.; Garcia de la Vega, J. M.; Claessens, C. G.; Poveda, L. A.; Gonzalez-Jonte, R. H. *J. Porphyrins Phthalocyanines* **2001**, *5*, 491.

(20) Ferro, V. R.; Garcia de la Vega, J. M.; Gonzalez-Jonte, R. H.; Poveda, L. A. *THEOCHEM* **2001**, *537*, 223.

(21) Ferro, V. R.; Poveda, L. A.; Gonzalez-Jonte, R. H.; Garcia de la Vega, J. M.; Torres, T.; del Rey, B. *J. Porphyrins Phthalocyanines* **2000**, *4*, 610.

(22) Martin, G.; Rojo, G.; Agullo-Lopez, F.; Ferro, V. R.; Garcia de la Vega, J. M.; Martinez-Diaz, M. V.; Torres, T.; Ledoux, I.; Zyss, J. *J. Phys. Chem. B.* **2002**, *106*, 13139.

(23) Yanagi, H.; Ikuta, K.; Mukai, H.; Shibutani, T. *Nano Lett.* **2002**, *2*, 951.

(24) Ohno-Okumura, E.; Sakamoto, K.; Urano, T. *Shikizai Kyokaishi* **2002**, *75*, 255.

(25) Suzuki, H.; Miki, H.; Yokoyama, S.; Mashiko, S. *J. Phys. Chem. B* **2003**, *107*, 3659.

(26) Zafirov, A.; Rakovski, S.; Bakardjieva-Eneva, J.; Prahov, L.; Assenova, L.; Marrandino, F. DVD-R optical recording medium using aluminum or boron subphthalocyanine and the method for the production thereof; Vivastar Mastering & Materials A.-G., Switz.; Application WO WO, 2002; 29 pp.

(27) Yamauchi, S.; Takahashi, A.; Iwasaki, Y.; Unno, M.; Ohba, Y.; Higuchi, J.; Blank, A.; Levanon, H. *J. Phys. Chem. A* **2003**, *107*, 1478.

(28) de Wild, M.; Berner, S.; Suzuki, H.; Yanagi, H.; Schlettwein, D.; Ivan, S.; Baratoff, A.; Guentherodt, H.-J.; Jung Thomas, A. *ChemPhysChem* **2002**, *3*, 881.

(29) Suzuki, H.; Berner, S.; Brunner, M.; Yanagi, H.; Schlettwein, D.; Jung, T. A.; Guntherodt, H. J. *Thin Solid Films* **2001**, *393*, 325.

(30) Mannsfeld, S.; Reichhard, H.; Fritz, T. *Surf. Sci.* **2003**, *525*, 215.

(31) Wang, Y.; Gu, D.; Gan, F. *Phys. Status Solidi A* **2001**, *186*, 71.

(32) Brunner, M.; Berner, S.; Jung, T. A.; Suzuki, H. Production method for atomic and molecular patterns on surfaces and nanostructured devices; Universitaet Basel, Switz.; Application: WO WO, 2002; 38 pp.

(33) Rauschnabel, J.; Hanack, M. *Tetrahedron Lett.* **1995**, *36*, 1629.

(34) Mastryukov, V.; Ruan, C.-y.; Fink, M.; Wang, Z.; Pachter, R. *J. Mol. Struct.* **2000**, *556*, 225.

(35) Ruan, C.-y.; Mastryukov, V.; Fink, M. *J. Chem. Phys.* **1999**, *111*, 3035.

(36) Claessens, C. G.; Gonzalez-Rodriguez, D.; del Rey, B.; Torres, T.; Mark, G.; Schuchmann, H.-P.; von Sonntag, C.; MacDonald, J. G.; Nohr, R. S. *Eur. J. Org. Chem.* **2003**, 2547.

(37) Zeil, W.; Haase, J.; Wegmann, L. *Z. Instrumentenkd.* **1966**, *74*, 84.

(38) Martinsen, K.-G.; Volden, H. V. Annual report from the Norwegian GED-Group, 1993.

(39) Martinsen, K.-G. Dissertation submitted to the Faculty of Matematics and Natural Sciences, University of Oslo, 1997.

(40) Gundersen, S.; Svein, S.; Strand, T. G.; Volden Hans, V. *J. Mol. Struct.* **2007**, *832*, 164.

(41) Gundersen, S.; Samdal, S.; Seip, R.; Strand, T. G. *J. Mol. Struct.* **2004**, *691*, 149.

(42) Ross, A. W.; Fink, M.; Hilderbrandt, R. *International Tables for Crystallography*; Wilson, A. J. C., Ed.; Kluwer Academic Publishers: Dordrecht, The Netherlands, 1992; Vol. C, p 245.

(43) Gundersen, G.; Samdal, S. Annual report from the Norwegian GED-Group, 1976.

(44) Frisch, M. J.; Trucks, G. W.; Schlegel, H. B.; Scuseria, G. E.; Robb, M. A.; Cheeseman, J. R.; Montgomery, J. A., Jr.; Vreven, T.; Kudin, K. N.; Burant, J. C.; Millam, J. M.; Iyengar, S. S.; Tomasi, J.; Barone, V.; Mennucci, B.; Cossi, M.; Scalmani, G.; Rega, N.; Petersson, G. A.; Nakatsuji, H.; Hada, M.; Ehara, M.; Toyota, K.; Fukuda, R.; Hasegawa, J.; Ishida, M.; Nakajima, T.; Honda, Y.; Kitao, O.; Nakai, H.; Klene, M.; Li, X.; Knox, J. E.; Hratchian, H. P.; Cross, J. B.; Adamo, C.; Jaramillo, J.; Gomperts, R.; Stratmann, R. E.; Yazyev, O.; Austin, A. J.; Cammi, R.; Pomelli, C.; Ochterski, J. W.; Ayala, P. Y.; Morokuma, K.; Voth, G. A.; Salvador, P.; Dannenberg, J. J.; Zakrzewski, V. G.; Dapprich, S.; Daniels, A. D.; Strain, M. C.; Farkas, O.; Malick, D. K.; Rabuck, A. D.; Raghavachari, K.; Foresman, J. B.; Ortiz, J. V.; Cui, Q.; Baboul, A. G.; Clifford, S.; Cioslowski, J.; Stefanov, B. B.; Liu, G.; Liashenko, A.; Piskorz, P.; Komaromi, I.; Martin, R. L.; Fox, D. J.; Keith, T.; Al-Laham, M. A.; Peng, C. Y.; Nanayakkara, A.; Challacombe, M.; Gill, P. M. W.; Johnson,

B.; Chen, W.; Wong, M. W.; Gonzalez, C.; Pople, J. A. *Gaussian 03*, Revision B.04; Gaussian, Inc.: Pittsburgh, PA, 2003.
(45) Hariharan, P. C.; Pople, J. A. *Mol. Phys.* **1974**, *27*, 209.
(46) McLean, A. D.; Chandler, G. S. *J. Chem. Phys.* **1980**, *72*, 5639.
(47) Krishnan, R.; Binkley, J. S.; Seeger, R.; Pople, J. A. *J. Chem. Phys.* **1980**, *72*, 650.
(48) Frisch, M. J.; Pople, J. A.; Binkley, J. S. *J. Chem. Phys.* **1984**, *80*, 3265.
(49) Dunning, T. H., Jr. *J. Chem. Phys.* **1989**, *90*, 1007.
(50) Becke, A. D. *J. Chem. Phys.* **1993**, *98*, 5648.
(51) Lee, C.; Yang, W.; Parr, R. G. *Phys. Rev. B* **1988**, *37*, 785.
(52) Ryeng, H.; Ghosh, A. *J. Am. Chem. Soc.* **2002**, *124*, 8099.
(53) Vangberg, T.; Lie, R.; Ghosh, A. *J. Am. Chem. Soc.* **2002**, *124*, 8122.
(54) Wasbotten, I. H.; Wondimagegn, T.; Ghosh, A. *J. Am. Chem. Soc.* **2002**, *124*, 8104.
(55) Ghosh, A. *J. Porphyrins Phthalocyanines* **2000**, *4*, 380.
(56) Nguyen, K. A.; Pachter, R. *J. Phys. Chem. A* **2000**, *104*, 4549.
(57) Parusel, A. B. J.; Wondimagegn, T.; Ghosh, A. *J. Am. Chem. Soc.* **2000**, *122*, 6371.
(58) Parusel, A. B. J.; Ghosh, A. *J. Phys. Chem. A* **2000**, *104*, 2504.
(59) Seip, H. M. *Specialist Periodical Reports*: *Molecular Structure by Diffraction Methods*; Sim, G. A., Sutton, L. E., Eds.; The Chemical Society: London, UK, 1973; Vol. 1, p 7.
(60) Kuchitsu, K. *Bull. Chem. Soc. Jpn.* **1967**, *40*, 498.
(61) Kuchitsu, K.; Morino, Y. *Bull. Chem. Soc. Jpn.* **1965**, *38*, 805.
(62) Almenningen, A.; Bastiansen, O.; Munthe-Kaas, T. *Acta Chem. Scand.* **1956**, *10*, 261.
(63) Almenningen, A.; Bastiansen, O.; Traetteberg, M. *Acta Chem. Scand.* **1961**, *15*, 1557.
(64) Almenningen, A.; Bastiansen, O.; Traetteberg, M. *Acta Chem. Scand.* **1959**, *13*, 1699.
(65) Morino, Y.; Nakamura, J.; Moore, P. W. *J. Chem. Phys.* **1962**, *36*, 1050.
(66) Morino, Y. *Acta Crystallogr.* **1960**, *13*, 1107.
(67) Hedberg, L.; Mills, I. M. *J. Mol. Spectrosc.* **1993**, *160*, 117.
(68) Hedberg, L.; Mills, I. M. *J. Mol. Spectrosc.* **2000**, *203*, 82.
(69) Sipachev, V. A. *THEOCHEM* **1985**, *22*, 143.
(70) Sipachev, V. A. *J. Mol. Struct.* **2001**, *567*−*568*, 67.